Journal of Vacuum Science and Technology B

RESEARCH ARTICLE | AUGUST 06 2021

Interferometric *in-situ* III/V semiconductor dry-etch depth-control with ±0.8 nm best accuracy using a quadruple-Vernier-scale measurement

Guilherme Sombrio ; Emerson Oliveira ; Johannes Strassner ; Christoph Doering ; Henning Fouckhardt

J. Vac. Sci. Technol. B 39, 052204 (2021)
https://doi.org/10.1116/6.0001209

JVST B
Journal of Vacuum Science & Technology B

ARTICLE

avs.scitation.org/journal/jvb

Interferometric *in-situ* III/V semiconductor dry-etch depth-control with ±0.8 nm best accuracy using a quadruple-Vernier-scale measurement

Cite as: J. Vac. Sci. Technol. B **39**, 052204 (2021); doi: 10.1116/6.0001209
Submitted: 12 June 2021 · Accepted: 20 July 2021 ·
Published Online: 6 August 2021

Guilherme Sombrio, Emerson Oliveira, Johannes Strassner, Christoph Doering, and Henning Fouckhardt[a)]

AFFILIATIONS

Research Group Integrated Optoelectronics and Microoptics (IOE), Physics Department, Technische Universität Kaiserslautern (TUK), PO Box 3049, D-67653 Kaiserslautern, Germany

[a)]**Author to whom correspondence should be addressed:** fouckhar@physik.uni-kl.de

ABSTRACT

Semiconductor multilayer and device fabrication is a complex task in electronics and opto-electronics. Layer dry etching is one of the process steps to achieve a specific lateral device design. *In situ and real-time monitoring* of etch depth will be necessary if high precision in etch depth is required. Nondestructive optical techniques are the methods of choice. Reflectance anisotropy spectroscopy equipment has been used to monitor the accurate etch depth during reactive ion etching of III/V semiconductor samples *in situ* and real time. For this purpose, temporal Fabry–Perot oscillations due to the etch-related shrinking thickness of the uppermost layer have been exploited. Earlier, we have already reported an etch-depth resolution of ±16.0 nm. By the use of a quadruple-Vernier-scale measurement and an evaluation protocol, now we even improve the *in situ* real-time etch-depth resolution by a factor of 20, i.e., nominally down to ±0.8 nm.

I. INTRODUCTION

Reactive ion etching (RIE) is widely applied in crystalline semiconductor technology, e.g., for the etching of multilayered III/V semiconductor samples like GaAs/$Al_xGa_{1-x}As$ heterostructures.[1–8] Usually, the etch process has to be stopped at a certain depth in order to meet the desired device design. For specific devices (see, e.g., Ref. 9), this might even require an etch-depth control with accuracies better than ±20 nm. However, this task cannot be met by the common approach to measure the etch depth *after* the completed etch process and *ex situ*. *In situ* real-time etch-depth monitoring and control is necessary for this purpose.

Reflectance anisotropy spectroscopy (RAS) equipment solves the problem. RAS is a nondestructive, optical, surface-sensitive technique originally developed to monitor epitaxial growth.[10–13] However, as this research group has already shown,[3–5,9,14] RAS can also be employed to monitor RIE of crystalline samples as long as the etch rate is not too large, i.e., as long as the sample surface (etch front) is not dismantled chaotically.

The genuine RAS signal is the photon energy $h\nu$-dependent difference ΔR in the optical reflectivity R (at normal light incidence) between two perpendicular directions x and y of linear polarization *along two main crystal axes*, normalized by the mean reflectivity $\langle R \rangle$,[11]

$$\frac{\Delta R}{\langle R \rangle}(h\nu) = \frac{R_x - R_y}{(R_x + R_y)/2}. \quad (1)$$

For normal incidence, a plane of incidence as well as parallel or perpendicular light polarization should not be definable. But clusters on the etch front break the symmetry and allow for reflectance differences for linearly polarized light depending on its plane of polarization.

However, not this basic RAS principle is used here but rather the RAS equipment with broadband (1.5–5.0 eV) light incidence perpendicular to the etch front. The occurrence of temporal Fabry–Perot oscillations (maxima = antiresonances due to the reflective setup) is exploited. They are due to the ever-shrinking thickness of

the uppermost layer. Their temporal period depends on photon energy and current etch rate (typically on the order of 70 nm/min). The oscillations can be observed either in the transients of the RAS signal for specific photon energies or in the so-called RAS color plot, which shows the temporal evolution of the RAS spectra with color-coded signal heights.

II. IMPROVING THE RESOLUTION OF ETCH-DEPTH MONITORING

In Ref. 9, we have shown that an etch-depth monitoring resolution of ±16.0 nm can be achieved using Fabry–Perot oscillations at one single photon energy. At that time, this value had already been an enormous improvement considering that the monitoring is performed *in situ* and in real time.

To achieve an even better accuracy/resolution, several periods of the Fabry–Perot oscillation would have to be measured. But this condition might not be satisfiable if the desired overall etch depth were not large enough. An alternative way is the evaluation of the oscillations for more than one photon energy or wavelength. In Ref. 14, we have already introduced the idea to use RAS *spectra* (i.e., to use more than one photon energy) and their temporal evolution in order to implement the optical/interferometric equivalent to a mechanical Vernier scale.[15,16]

The Fabry–Perot oscillations can be observed in the color plot—see, e.g., Fig. 1 for the case of a sequence of $Al_{0.5}Ga_{0.5}As$ layers interspersed with GaAs layers. The abscissa is made of the photon energy, and the ordinate is represented by the time along the etch process.

As can be deduced from Fig. 1, as expected, the Fabry–Perot oscillations have slightly different temporal periods depending on photon energy, since the quotient

$$\frac{2d(\Delta t)}{\lambda_0/n} = 2d(\Delta t)\frac{h\nu}{hc/n} \tag{2}$$

is dependent on photon energy $E = h\nu$ or vacuum wavelength $\lambda_0 = hc/E$. The etch time-dependent quantity $d(\Delta t)$ represents the current, momentarily remaining thickness of the uppermost layer, Δt represents the etch duration starting with $t = 0$ at the original top layer interface, n stands for the refractive index (which itself is dependent on photon energy or wavelength), λ_0/n is the wavelength within the semiconductor layer, ν represents the light frequency, c is the vacuum phase velocity of light, and h is Planck's constant.

The quotient, according to Eq. (2), gives the number of times the material wavelength λ_0/n fits into the round-trip length ($2d$) of the top layer considered as a Fabry–Perot resonator and, hence, determines reflectivity.

For two different photon energies or wavelengths, the temporal Fabry–Perot oscillation period $T(h\nu) = T(\lambda_0)$ is slightly different, such that temporal oscillations (or their spatial equivalent in the RAS color plot) can be regarded as two "rulers" with slightly different scale divisions. This is the reason why we call it a Vernier-scale like measurement.

In Ref. 14 this way, we have improved *in situ* real-time etch-depth resolution from ±16.0 nm down to a value of ±3.5 nm by a single Vernier scale (i.e., use of second photon energy), which nominally amounts to ±6.2 lattice constants for our material system, i.e., AlGaAs.

This contribution goes a step further by optimizing the measurement and evaluation procedure in several regards. First, we use five different photon energies or wavelengths instead of just two to improve resolution in general once more. One might consider this as one measurement plus the usage of four Vernier scales simultaneously. Furthermore, to be able to stop an etch process at a specific etch depth with the desired accuracy, it is important to computer-calculate the etch rate along with the evolvement of Fabry–Perot oscillations. The etch rate calculations are done with increasing accuracy—considering the increments of half an oscillation period—after ½T, 1T, 1½T, and so on.

With current etch depth $\Delta d(\Delta t)$ and etch duration Δt so far, the etch rate r is

$$r = \frac{\Delta d(\Delta t)}{\Delta t} = \frac{\lambda_0}{[2n(\lambda_0)]\,T(\lambda_0)}. \tag{3}$$

The factor of 2 is important, since the light is going forth and back through the remaining layer thickness. In the case of any one oscillation period T, the light path forth and back amounts to *one wavelength* $\lambda = \lambda_0/n$ *less* inside the material of the top layer. In that case, the layer has only been etched by an additional amount equivalent to $\lambda/2$.

With the retrieved etch rate r, it is easy to calculate the current/momentary etch depth

$$\Delta d(\Delta t) = r \cdot \Delta t = \frac{\lambda_0}{2 \cdot n \cdot T} \cdot \Delta t \tag{4}$$

successively better and using interpolation over time. The ever

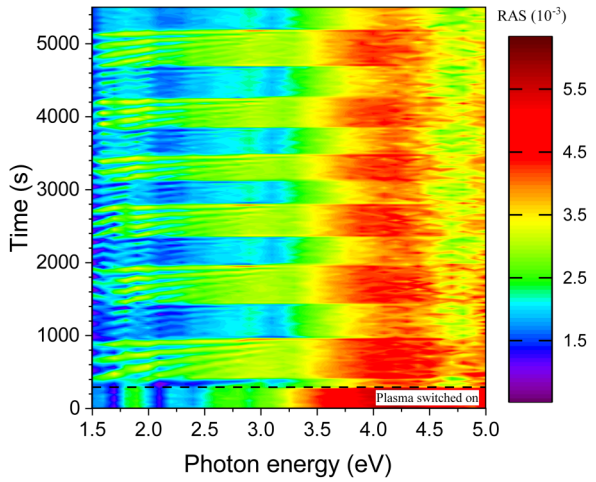

FIG. 1. Temporal evolution of RAS spectra (leading to the color plot) acquired during an RIE process for a sequence of $Al_{0.5}Ga_{0.5}As$ layers interspersed with GaAs layers. The RAS signal height is color-coded as the scale on the right suggests.

more accurately deduced etch rate value results in an ever more accurately retrieved value of the current etch depth.

For most RIE applications, an accuracy reached after one oscillation period T corresponding to an additional etch depth of $\lambda/2$ will suffice. But even when a resolution better than ±2.0 nm is desired, an etch duration of not more than about 1½ T should suffice for adequate interpolation—equivalent to an overall etch depth of ¾ λ—as we will show. Typical overall etch depths in semiconductor technology are larger so that this condition does not represent any restriction.

Statistical analysis is applied to increase accuracy. This way, we have finally come to an etch-depth monitoring resolution of ±0.8 nm in the best case, which nominally amounts to ±1.4 lattice constants in our material system AlGaAs with a lattice constant of 0.565 nm.

III. MATERIALS, EQUIPMENT, AND ADJUSTMENT

The multilayered samples used further-on for this contribution have been prepared by molecular beam epitaxy (MBE) in an R450 MBE system from DCA Instruments Oy, Turku, Finland. Each 2-in. GaAs substrate has been overgrown with a GaAs buffer as well as six subsequent layers made from $Al_{0.5}Ga_{0.5}As$ (so-called layer VI—layer numbers chosen for sequence upon etching), GaAs (V), $Al_{0.5}Ga_{0.5}As$ (IV), GaAs (III), $Al_{0.5}Ga_{0.5}As$ (II), and GaAs (I) to be observed in the scanning electron microscope (SEM) image of Fig. 2 with a perpendicular electron beam incidence onto the sample side facet. The layer thicknesses given in the micrograph correspond to one measurement sequence for this unetched sample at one site on the facet. In Table I, layer thicknesses are given for this sample/wafer but averaged over several measurement sequences at different sites on the facet. Those values have an uncertainty of ±6%.

After the epitaxial process, the wafer has been diced/cleaved into several pieces of 8 mm^2. The reactive ion dry-etch process is performed in a parallel plate reactor MicroSys 350 from Roth & Rau, Wuestenbrand, Germany using a bias voltage of 500 V. The plasma contains a gas mixture of Ar (50 sccm) and Cl_2 (1 sccm). The pressure is adjusted to a value between 9.0×10^{-3} and 9.8×10^{-3} hPa.[17]

The *in situ* real-time measurements are pursued using the standard EpiRAS system manufactured by Laytec, Berlin, Germany. The range of photon energies of the RAS system extends from 1.5 to 5.0 eV with minimum steps of 0.05 eV. The RAS system is positioned above a viewport, which itself is perpendicular above the sample surface in the RIE machine. Before the etch process, the RAS system is rotated by hand around its optical axis to maximize the RAS signal and fixed for that orientation. This is the case when the direction of linear light polarization forms an angle of 45° to two main crystal axes of the cubic α zinc blende crystal [called x and y before; for (001) wafer surfaces as in our case these crystal axes are the [110] axis and the [−110] axis].

Depending on exact conditions (etch parameters and material composition), sometimes the genuine RAS signal according to Eq. (1) shows Fabry–Perot oscillations with strong modulation/contrast, and sometimes this is rather true for mean reflectivity $\langle R \rangle$ [the denominator in Eq. (1)].

TABLE I. Thicknesses of the III/V layers of the crystalline multilayered sample from Fig. 2; the thicknesses are obtained (and averaged) from several SEM measurement sequences on different facet sites; the accuracy of these values is better than ±6%, i.e., better than ±19 nm.

Layer thickness (nm)	
I—GaAs cap	325.0
II—$Al_{0.5}Ga_{0.5}As$	325.6
III—GaAs	309.7
IV—$Al_{0.5}Ga_{0.5}As$	331.8
V—GaAs	326.7
VI—$Al_{0.5}Ga_{0.5}As$	329.5

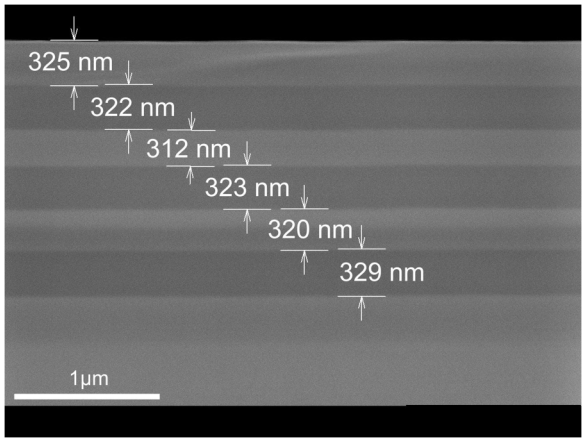

FIG. 2. SEM micrograph showing a perpendicular facet view of one sample and the measured values for a single site on the facet (top layer = layer I, bottom = VI).

IV. DATA RETRIEVAL AND EVALUATION

The refractive indices of the semiconductor layer materials are essential to calculate the current etch-depth accurately by Eq. (4). Figure 3 gives the wavelength $\lambda = \lambda_0/n$ within the semiconductor material (the so-called material wavelength) for GaAs and

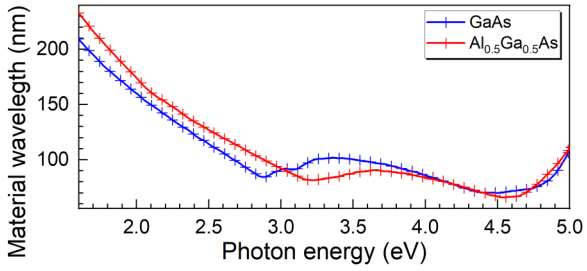

FIG. 3. Material wavelength λ as a function of photon energy $h\nu$ for GaAs and $Al_{0.50}Ga_{0.50}As$ using refractive index values extracted from Ref. 18.

$Al_{0.50}Ga_{0.50}As$ as a function of photon energy, and the refractive indices are taken from the literature.[18]

Considering the monitoring accuracy, the wavelength should be as small as possible. But in order to have Fabry–Perot oscillations appear, the light penetration depth should be large enough, and absorption by the semiconductor material should be small enough. These arguments advocate a relatively large wavelength or small photon energy.

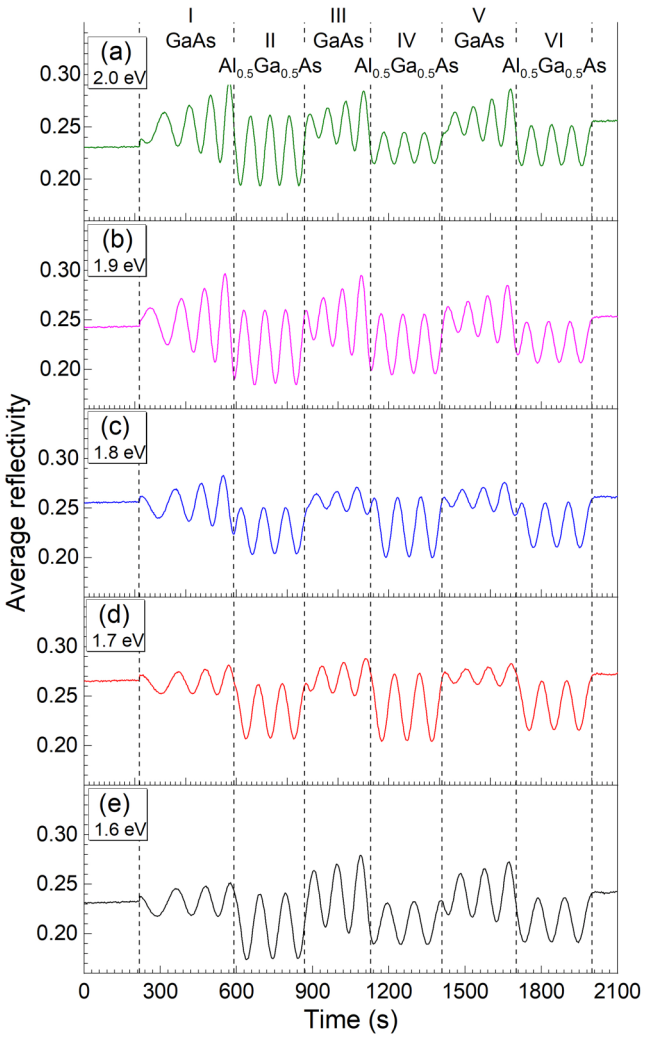

FIG. 4. Transients of the average reflectivity $\langle R \rangle$ of the GaAs/$Al_{0.50}Ga_{0.5}As$ multilayered sample etched by RIE acquired with photon energies at (a) 2.0, (b) 1.9, (c) 1.8, (d) 1.7, and (e) 1.6 eV. The plasma has been switched on at 215 s after the start of data collection and—in this case—kept on until all layers have been etched completely. For the GaAs layers (direct bandgap of 1.44 eV), the oscillation amplitude is lowest for the still relatively thick layers and increases with etch time, because absorption at photon energies at 1.6–2.0 eV has less and less influence along etching of these layers. For $Al_{0.50}Ga_{0.5}As$ layers, (indirect bandgap of about 1.80 eV), this issue is much less important and the oscillation amplitude nearly stays constant upon etching of these layers.

For samples of our material system, we usually observe Fabry–Perot oscillations best for photon energies around 2 eV in the sense that the modulation/contrast of the oscillations is best then.

Figure 4 illustrates the transients of the average reflectivity of one of the multilayered GaAs/$Al_{0.5}Ga_{0.5}As$ samples (from the same wafer). The signals have been acquired at five different photon energies in the range of 1.6–2.0 eV with a step size of 0.1 eV, which, of course, corresponds to five different wavelengths. The plasma has been ignited (switched-on) at 215 s after the beginning of data collection marked with the left-most black dashed line in Fig. 4. The oscillatory temporal evolution of the signal reveals the reduction in layer thickness and the shrinking Fabry–Perot resonator length. The GaAs cap layer (layer I to be etched) is completely etched away within the first 380 s of the etch process (up to 215 + 380 s = 595 s after the beginning of data collection). The encounters of interfaces between layers upon continued etching are observable in the transients by slope discontinuities, marked with additional black dashed lines in Fig. 4. The slope discontinuities have their origin in refractive index changes from one layer to the next.

For the GaAs layers (direct bandgap energy of 1.44 eV), the oscillation amplitude is lowest for the still relatively thick layers and increases with etching time because absorption at photon energies between 1.6 and 2.0 eV has less and less influence along the etch time. For the $Al_{0.50}Ga_{0.5}As$ layers (indirect bandgap energy of about 1.80 eV), this issue is much less important, and the oscillation amplitude nearly stays constant upon etching of these layers, even for photon energies $\geq$1.8 eV.

In the etch process related to Fig. 4, the semiconductor layers have been etched completely. Thus, the final etch depths correspond to the total thicknesses of these layers. In this case, $\Delta t = \Delta t_{complete}$ from Eqs. (3) and (4) stands for the time interval between the beginning and the end of the etch duration for each of the layers.

Moreover, calculations are performed for temporal increments corresponding to steps of half a Fabry–Perot oscillation period, i.e., for $\Delta t = \frac{1}{2}T$, $1T$, $1\frac{1}{2}T$, and $2T$ for layers V and VI. The quantity Δd ($\Delta t_{complete}$) is calculated with its mean value and standard deviation for all five photon energies and for any of the temporal increments.

For instance, $\frac{1}{2}T$ is taken from the first half period (e.g., maximum to minimum or vice versa) of the transients as well as $\Delta t_{complete}$ for one photon energy for the completion of the layer etch (marked by the black dashed lines in Fig. 4). From this, the etch rate r is calculated with Eq. (3), and the full layer thickness $d = \Delta d_{complete} = \Delta d_{maximum}$ is estimated with Eq. (4) and using $\Delta t_{complete}$. Then, the layer thickness is calculated following the same procedure for another of the five photon energies considering the same half period and so on for the third, fourth, and fifth photon energy. Mean values and standard deviations of d are calculated for all five chosen photon energies for the first half period. Then, the next five calculations are performed for $1T$, which means to take the first complete period of the transients and so on.

Figure 5, made for the etching of layer VI ($Al_{0.5}Ga_{0.5}As$), shows the time evolution of the interpolation of Δd (etch depth), where each panel of the figure corresponds to results achieved for one more half period of the Fabry–Perot oscillation as described above. It is important to mention that—as expected—the error bars

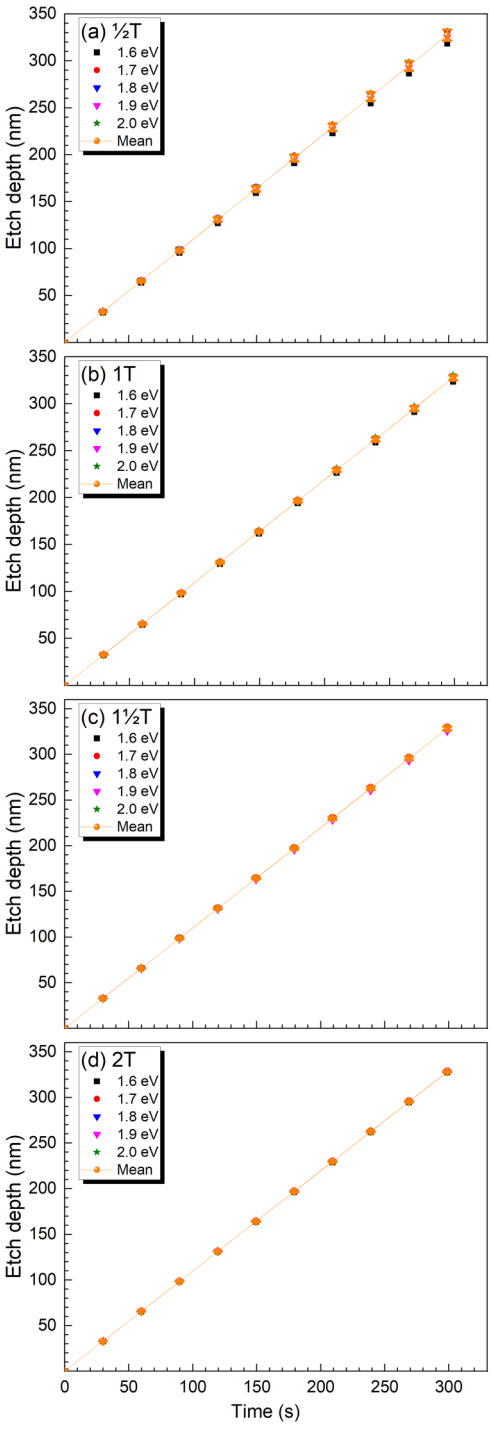

FIG. 5. Interpolation of etch depth for layer VI ($Al_{0.5}Ga_{0.5}As$) as a function of time calculated considering temporal increments corresponding to steps of half a Fabry–Perot oscillation period: (a) ½T, (b) 1T, (c) 1½T, and (d) 2T. The mean values have been calculated considering the five photon energies for each panel.

TABLE II. Thickness *d* of the layers V (GaAs) and VI ($Al_{0.5}Ga_{0.5}As$) measured by SEM (just the first data line boldface and italic) and calculated according to Eq. (4) and the measured Fabry–Perot oscillations in steps of *T*/2 (lines 2–5).

Thickness *d* of the layers (nm)		
Layer	V—GaAs	VI—$Al_{0.5}Ga_{0.5}As$
SEM	***326.7 ± 7.0***	***329.5 ± 6.8***
½T	326.8 ± 5.9	331.0 ± 5.8
1T	325.7 ± 3.7	328.1 ± 2.6
1½T	325.1 ± 1.6	329.3 ± 2.0
2T	326.6 ± 1.8	328.3 ± 0.8

become smaller with the increments of half an oscillation period. Moreover, the constancy of the etch rate is evident from the nearly perfect linearity of the curves. The same type of calculations has been performed for layer V, but those results are not given in Fig. 5.

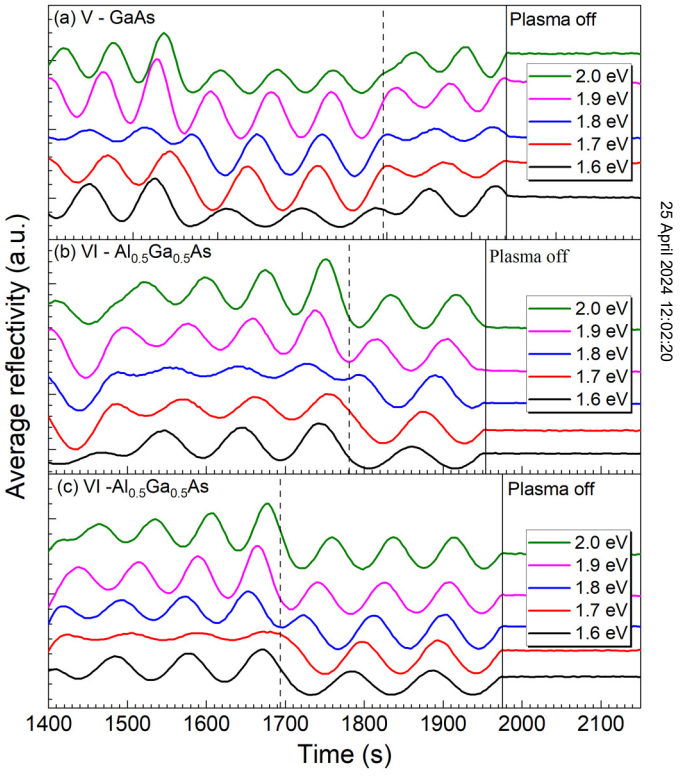

FIG. 6. Transients of average reflectivity for three independent etch processes and five photon energies in each case. *In each diagram, the five curves for the five photon energies are slightly shifted along the ordinate with respect to one another in order to give a better visualization.* The etch processes have been stopped at three different points: in layer (a) V (GaAs), (b) VI ($Al_{0.5}Ga_{0.5}As$), and (c) VI ($Al_{0.5}Ga_{0.5}As$). Black dashed lines point to the beginning of the etching of the specific layer under consideration, while black solid lines mark the moment when the plasma is switched off, thus ending the etch process.

TABLE III. Etch-depth estimation (NA = not applicable = not enough half periods have emerged upon etching due to a shallow etch).

	Etch depth estimation (nm)		
Layer	(a) V—GaAs	(b) VI—$Al_{0.5}Ga_{0.5}As$	(c) VI—$Al_{0.5}Ga_{0.5}As$
½T	189.7 ± 2.2	182.0 ± 5.1	304.1 ± 3.9
1T	189.9 ± 3.2	183.6 ± 1.9	301.7 ± 3.4
1½T	190.5 ± 1.6	NA	302.5 ± 2.1
2T	NA	NA	301.9 ± 1.0

The first data line of Table II shows the total layer thicknesses d of layers V and VI measured with the help of scanning electron microscope (SEM) images of the sample side facets (see explanations further above). And lines 2–5 of the same table give the thicknesses calculated according to the procedure reported above. The values have less than 0.5% difference to the bench-mark mean value achieved by SEM.

The standard deviation is as low as ±0.8 nm in the best case, giving a tolerance range of 2·0.8 nm = 1.6 nm (with 68.3% probability), as long as the number of overall Fabry–Perot periods is $\geq 2T$, that is, when two Fabry–Perot oscillation periods or more are taken into account.

It is important to stress that this high accuracy is possible because the measurements and evaluation calculations are performed for five photon energies. This means that not just one and not just two "rulers" (as for a conventional Vernier scale setting) are used, but rather five "rulers" with their slightly different scales. If a weaker resolution is acceptable, the use of two different photon energies might suffice.

V. FURTHER CHECK OF APPLICABILITY OF THE PROCEDURE

To check the practical applicability of this technique even further, three more samples (cleaved from a single epitaxially overgrown MBE wafer), each with about 8 mm^2 surface area, have been etched separately. The three etch processes have been stopped at different etch depths inside layer V (GaAs) or layer VI ($Al_{0.5}Ga_{0.5}As$). Figure 6 illustrates the recorded transients (five for five photon energies again) in each of the three etch processes. The black dashed lines mark the beginning of the etching of the relevant layer, while the black solid lines mark the end of etching at plasma switch-off.

The calculated mean etch-depths along with their standard deviations are given in Table III. As expected, the latter decrease with increments of half a Fabry–Perot oscillation period. This time the standard deviations are not as low as ±0.8 nm. But even in case (c) with only 1½ T (due to a shallow etch), the standard deviation is as low/good as ±2.1 nm, which is by far sufficient for any modern dry-etch process.

VI. CONCLUSIONS

RAS *equipment* is used to monitor and control III/V semiconductor etch depths during RIE processes with high precision. For this purpose, the Fabry–Perot oscillations in the signal transients at photon energies around 2 eV are evaluated. To improve accuracy or resolution—even for small intended overall etch-depths—more than one photon energy is employed. The oscillation periods for different photon energies are slightly different, thus providing for different "rulers" and a multiple Vernier-scale like measurement protocol.

We have used five photon energies (1.6, 1.7, 1.8, 1.9, and 2.0 eV). The best achieved standard deviation for etch depth amounts to ±0.8 nm. But even for less extreme settings and the extraction of no more than 1.5 or 2 Fabry–Perot oscillation periods in cases of shallow etching, standard deviations on the order of just a few nanometers are possible this way. Probably in everyday work, it will be more of a problem to take the time delay between the computer command to switch off the plasma and the actual switch off into account accurately.

RAS equipment, in combination with the multiple Vernier-scale like interferometric measurement and evaluation procedure, is a powerful tool for precise *in situ* real-time dry-etch depth control.

ACKNOWLEDGMENTS

The project has been funded by the German Research Foundation (DFG, Deutsche Forschungsgemeinschaft) under Contract Nos. FO157/58-1 and FO157/63-1. The research group is a member of the users' group of the Nano Structuring Center (NSC) of the Technische Universität Kaiserslautern (TUK) and is thankful for general NSC assistance.

DATA AVAILABILITY

The data that support the findings of this study are available from the corresponding author upon reasonable request.

REFERENCES

[1]F. Karouta, J. Phys. D: Appl. Phys. **47**, 233501 (2014).
[2]C. Doering, A.-K. Kleinschmidt, L. Barzen, H. Fouckhardt, M. Wahl, and M. Kopnarski, "*In-situ* plasma etch depth control with reflectance anisotropy spectroscopy (RAS)," in *Micro-Nano-Integration. 6. GMM-Workshop* Duisburg, October 5th and 6th (VDE-GMM, Frankfurt/Main, Germany, 2016).
[3]C. Doering, A.-K. Kleinschmidt, L. Barzen, J. Strassner, and H. Fouckhardt, "Atomic layer sensitive *in-situ* plasma etch depth control with reflectance anisotropy spectroscopy (RAS)," in *Proceedings SPIE 10329 Optical Measurement Systems for Industrial Inspection X*, Munich, 26 June 2017 (SPIE Europe, Ffordd Pengam, Cardiff, Wales, 2017). doi:10.1117/ 12.2269708.
[4]L. Barzen, A.-K. Kleinschmidt, J. Strassner, C. Doering, H. Fouckhardt, W. Bock, M. Wahl, and M. Kopnarski, Appl. Surf. Sci. **357**, 530–538 (2015).
[5]L. Barzen, J. Richter, H. Fouckhardt, M. Wahl, and M. Kopnarski, Appl. Surf. Sci. **328**, 120–124 (2015).
[6]A. R. Heyd, R. W. Collins, K. Vedam, S. S. Bose, and D. L. Miller, Appl. Phys. Lett. **60**, 2776–2778 (1992).
[7]A. R. Heyd, I. An, R. W. Collins, Y. Cong, K. Vedam, S. S. Bose, and D. L. Miller, Film **9**, 810–815 (1991).
[8]J. Y. Shin, K. H. Choi, K. H. Noh, D. K. Park, K. Y. Sohn, G. S. Cho, H. J. Song, J. W. Lee, and S. J. Pearton, Thin Solid Films **521**, 245–248 (2012).
[9]A.-K. Kleinschmidt, L. Barzen, J. Strassner, C. Doering, H. Fouckhardt, W. Bock, M. Wahl, and M. Kopnarski, Beilstein J. Nanotechnol. **7**, 1783–1793 (2016).
[10]C. Meyne, M. Gensch, S. Peters, U. W. Pohl, J.-T. Zettler, and W. Richter, Thin Solid Films **364**, 12–15 (2000).

[11]P. Weightman, D. S. Martin, R. J. Cole, and T. Farrell, Rep. Prog. Phys. **68**, 1251–1341 (2005).
[12]J. Ortega-Gallegos, L. E. Guevara-Macías, A. D. Ariza-Flores, R. Castro-García, L. F. Lastras-Martínez, R. E. Balderas-Navarro, R. E. López-Estopier, and A. Lastras-Martínez, Appl. Surf. Sci. **439**, 963–967 (2018).
[13]V. L. Berkovits and D. Paget, Thin Solid Films **233**, 9–13 (1993).
[14]C. Doering, J. Strassner, and H. Fouckhardt, AIP Adv. **9**, 075116 (2019).
[15]K. A. Stetson, "Method for measurement of surface profile change using a vernier scale in hologram interferometry," U.S. patent 36,126,93A (1971), see https://patents.google.com/patent/US3612693A/en
[16]A. G. Kwan, Am. J. Phys. **79**, 368–373 (2011).
[17]A. G. Laytec, see https://www.laytec.de/epiras/ for EpiRAS TT, Berlin, Germany (accessed November 10, 2020).
[18]D. E. Aspnes, S. M. Kelso, R. A. Logan, and R. Bhat, J. Appl. Phys. **60**, 754–767 (1986).